Electronic Supplementary Material (ESI) for Journal of Materials Chemistry A.

Supporting Information

Boosting the Pseudocapacitance of Nitrogen-rich Carbon Nanorod Arrays for Electrochemical Capacitors

Duo Yang, Yu Song*, Yin-Jian Ye, Mingyue Zhang,Xiaoqi Sun, Xiao-Xia Liu*

Department of Chemistry, Northeastern University, Shenyang, 110819, China

Corresponding author:

Yu Song, songyu@mail.neu.edu.cn

Xiao-Xia Liu, xxliu@mail.neu.edu.cn

Calculations

1. Calculation of single electrode:

The gravimetric capacitance (C_m) of a single electrode can be calculated from constant current charge-discharge profile according to the following equation:

$$C_m = \frac{I \times \Delta t}{\Delta U \times m} \text{(Equation S1)}$$

where C_m (F g^{-1}) is the gravimetric capacitance, I (mA)is the discharge current, Δt (s)is the time, ΔU (V)is the potential window, m (mg) is the mass of active material.

2. Calculations for the device:

The gravimetric capacitance (C_M) of the NP350//NP350 device can be calculated based on constant current charge-discharge profile according to the following equation:

$$C_M = \frac{I \times \Delta t}{\Delta U \times M} \text{ (Equation S2)}$$

where C_M (F g^{-1}) is the gravimetric capacitance of the device, I (mA)is the discharge current, Δt (s) is the time, ΔU (V) is the operating voltage of the device, M (mg) is the total mass of active material.

Energy density (E, Wh/kg) and power density (P, kW/kg) can be calculated according to the following equations:

$$E = \frac{1000 \times C \times U^2}{2 \times 3600} \text{ (Equation S3)}$$

$$P = \frac{3600 \times E}{t} \text{ (Equation S4)}$$

Where C(F g^{-1}) is the volumetric capacitance, U(V) is the operating voltage and t (s) is the discharge time.

Supplementary Figures

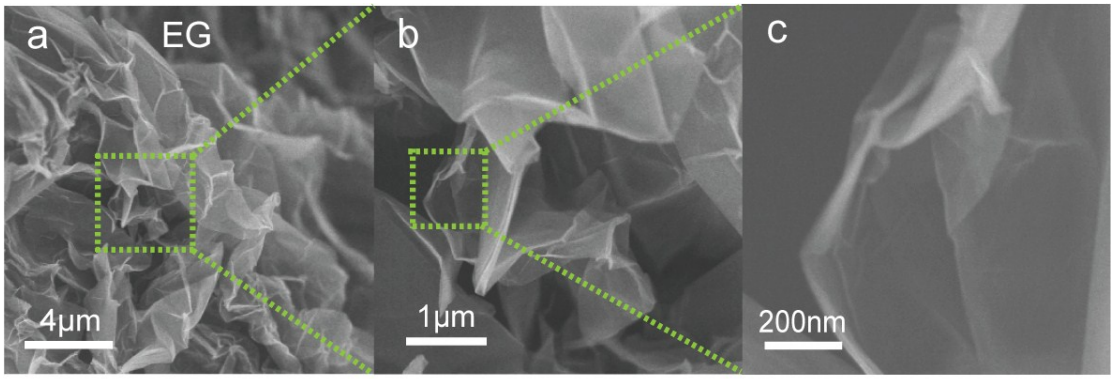

Figure S1 SEM images of the 3D exfoliated graphite current collector (EG).

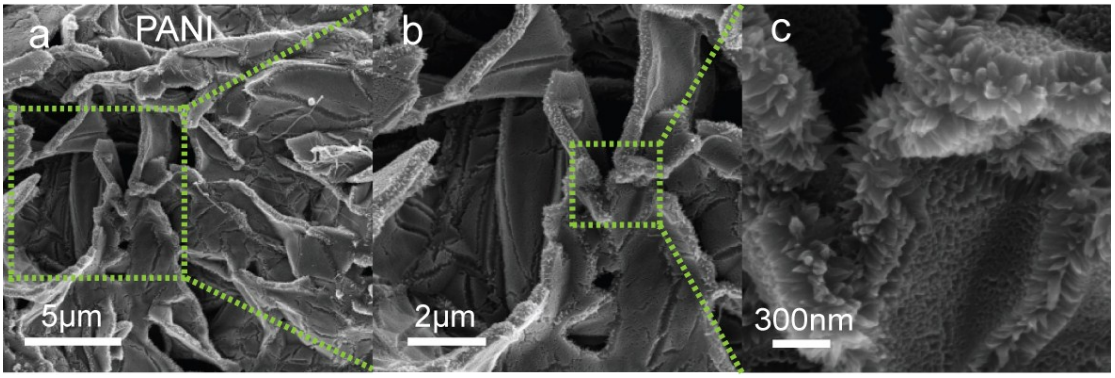

Figure S2 SEM images of PANI/EG sample.

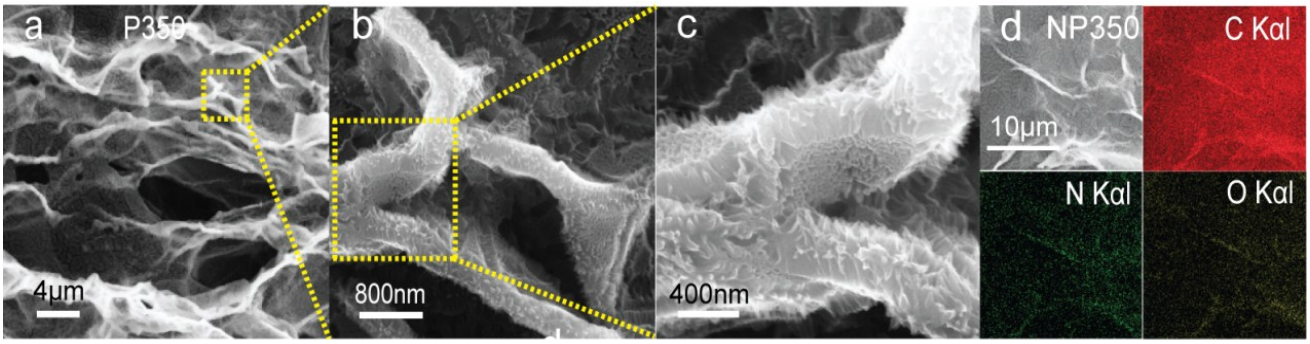

Figure S3 (a, b, and c) SEM images of P350 sample. (d) SEM image of NP350 and corresponding elemental mapping images of C, N and O.

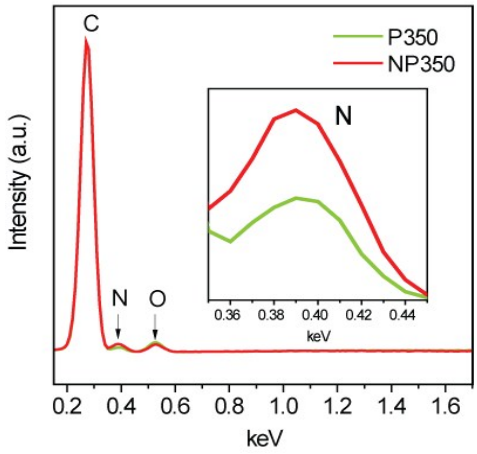

Figure S4 The EDS data of P350 and NP350. Inset shows the enlarged N signal.

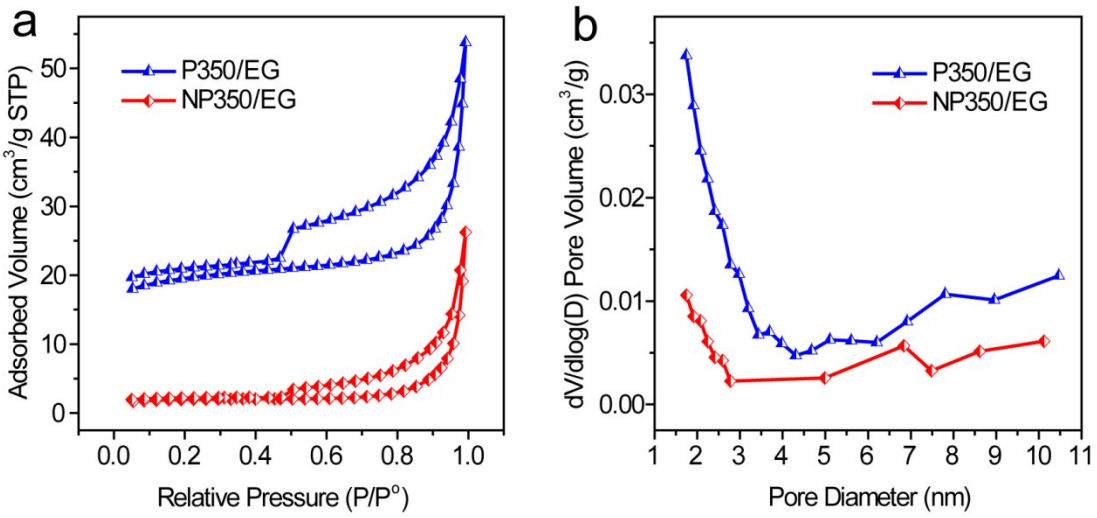

Figure S5 (a) Nitrogen adsorption-desorption isotherms and (b) pore-size distribution plots of P350 and NP350 samples.

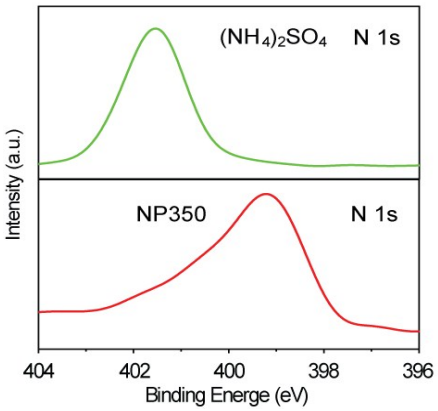

Figure S6 N 1s core level XPS spectra of $(NH_4)_2SO_4$ and NP350 samples.

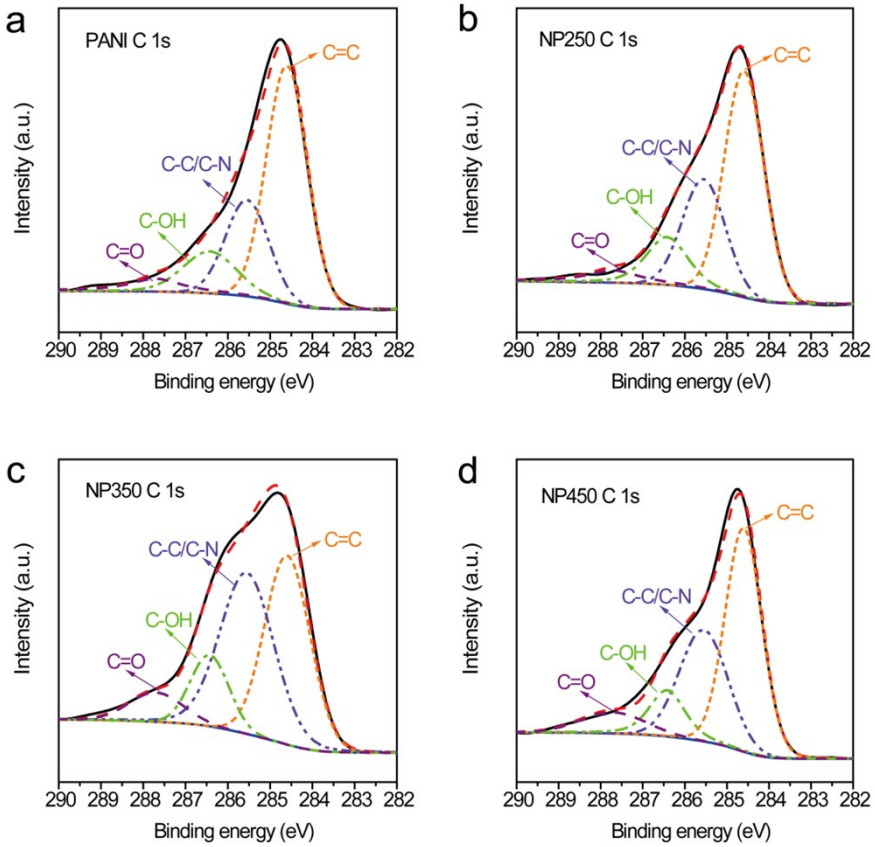

Figure S7 C 1s core-level XPS spectra of PANI, NP250, NP350, and NP450 samples.

The C 1s spectra can be divided into four peaks centered at ~ 284.59 eV (C=C), 285.55 eV (C-C and C-N), 286.42 eV (C-OH), and 287.70 eV (C=O). [1] The different C 1s spectra of samples indicate the gradual evolution of the material during the annealing treatment at different temperature.

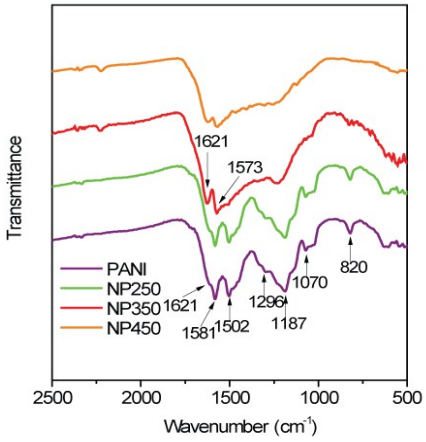

Figure S8 FT-IR spectra of PANI, NP250, NP350 and NP450 samples.

In the FT-IR spectrum of PANI sample, the typical characteristic peaks of polyaniline can be obviously observed. The peaks at 1581 cm^{-1} and 1502 cm^{-1} are related to stretching vibration of quinoid and benzenoid rings in PANI chains.[2, 3] The C–N stretch of benzenoid is located at 1296 cm^{-1}, while the N=Q=N stretch of the quinoid ring is observed at 1187 cm^{-1}. The peaks at 1070 cm^{-1} and 820 cm^{-1} can be ascribed to C-H stretch of aromatic ring.[4]

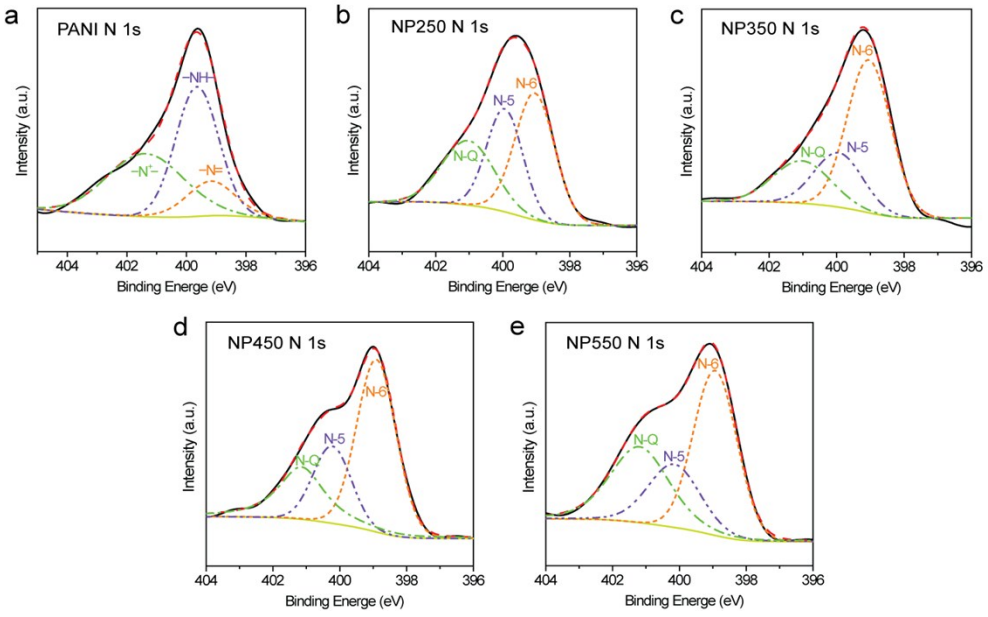

Figure S9 N 1s core-level XPS spectra of PANI, NP250, NP350, NP450 and NP550 samples.

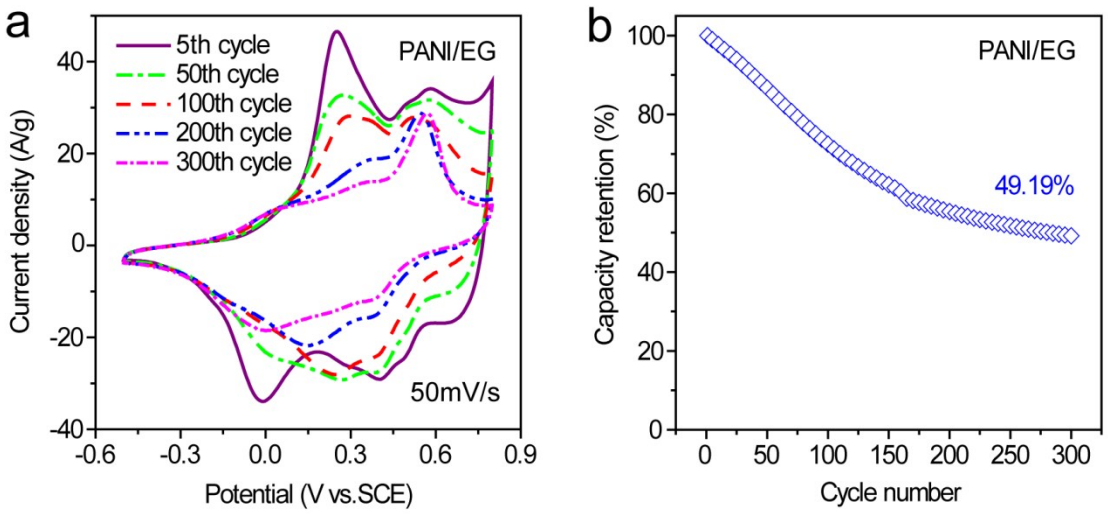

Figure S10 (a) CV curves of PANI at different cycles. (b) Capacitance retention of PANI electrode at a scan rate of 50mV s^{-1} in 300 cycles.

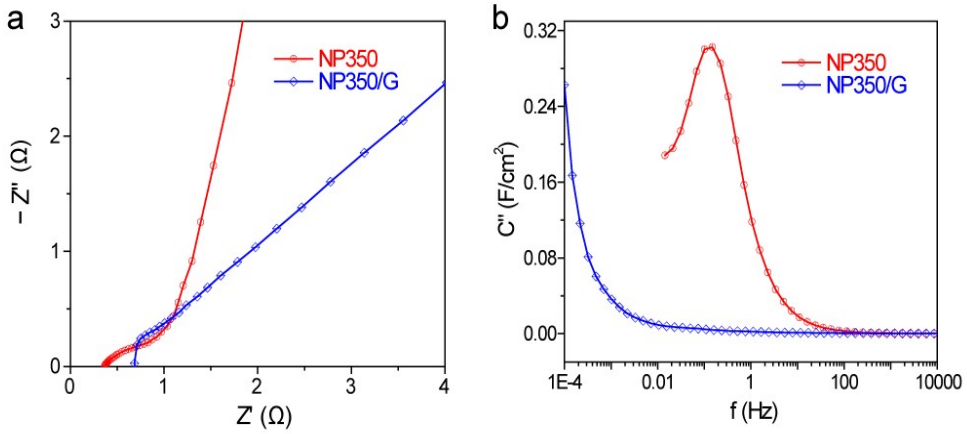

Figure S11 (a) Nyquist plots for NP350/G and NP350. (b) Plots of C" as a function of frequency for NP350/G and NP350.

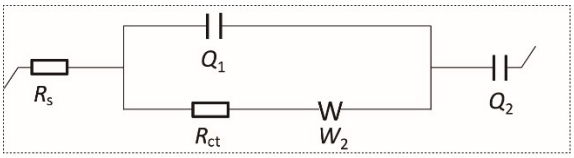

Sample	R_s	R_{ct}	W
NP350	0.357	0.693	0.642
NP350/G	0.678	5.678	35.15

Figure S12 The equivalent circuit diagram and the corresponding fitting values.

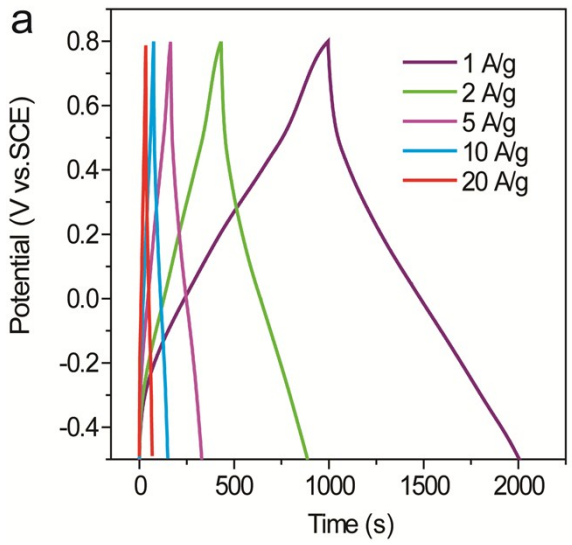

Figure S13 The galvanostatic charge/discharge curves ofNP350 sample at different current densities.

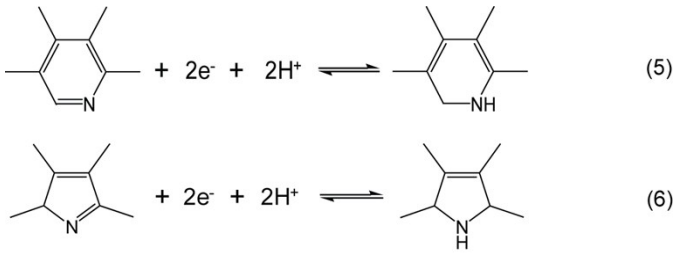

Figure S14 The redox processes of N-6, N-5 in H_2SO_4 electrolyte.

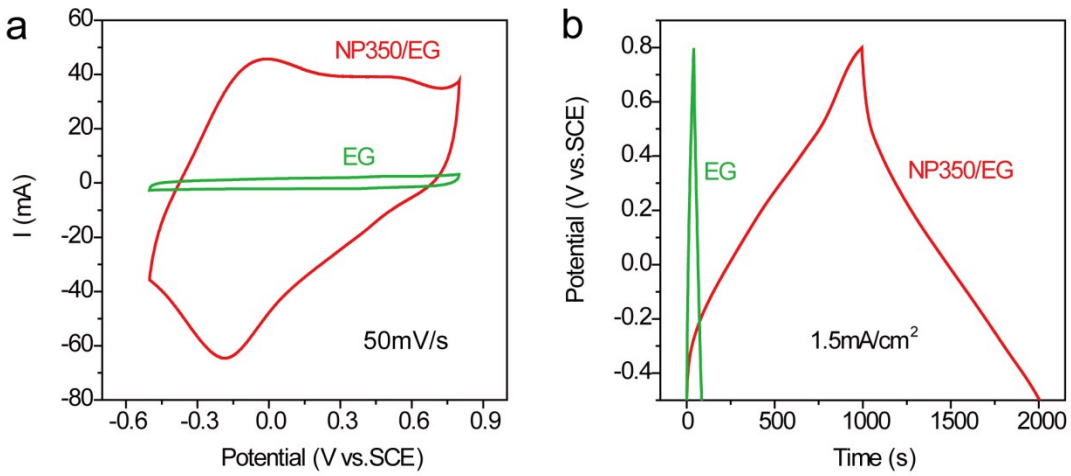

Figure S15 (a) CV curves and (b) the galvanostatic charge/discharge curves of NP350/EG and EG.

The nanorod arrays were uniformly coated on the graphite/graphene surface, so that the majority of the substrate was not in contact with the electrolyte. Therefore, the carbonaceous nanorod arrays are mainly responsible for the capacitance of the composite electrode, while the contribution from EG is much smaller than the case of bare EG and could be ignored.

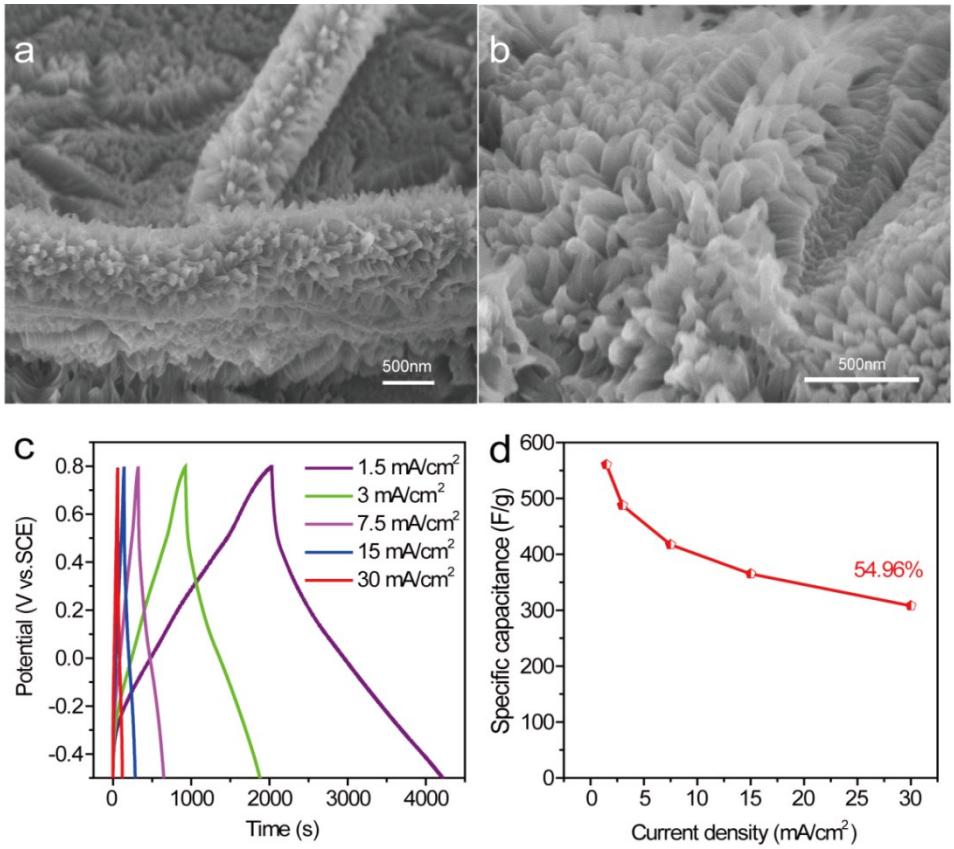

Figure S16 (a, b) SEM images of the high mass loaded NP350 sample. (c) The galvanostatic charge/discharge curves of the high mass loaded NP350 sample. (d) Specific capacitances of the electrode obtained at different current densities.

Table S1. Electrochemical performances of the reported nitrogen-doped carbon materials.

Materials	Mass loading	Capacitance (Max.)	Capacitance (Min.)	Cycling stability
Hierarchical porous N,O,S-enriched carbon	1.32 mg cm^{-2}	402.5 F g^{-1} (1 A g^{-1})	371.5 F g^{-1} (10A g^{-1})	90% after 20000 cycles[1]
Porous carbon foam	2.5 mg cm^{-2}	382.4 F g^{-1} (1 A g^{-1})	335.5F g^{-1} (40 A g^{-1})	98% after 20000 cycles[5]
Nitrogen and sulfur codoped graphene	1.0mg cm^{-2}	281 F g^{-1} (1 A g^{-1})	199 F g^{-1} (10 A g^{-1})	95.4% after 6000 cycles[6]
Nitrogen-doped porous carbon	2.0 mg cm^{-2}	321.7 F g^{-1} (1 A g^{-1})	165.35 F g^{-1} (20 A g^{-1})	100% after 20000 cycles[7]
Nitrogen and oxygen dual-doped carbon	0.1 mg cm^{-2}	251 F g^{-1} (0.5 A g^{-1})	170 F g^{-1} (30 A g^{-1})	99.5% after 10000 cycles[8]
Aminophenyl multiwall carbon nanotube	2.5-3 mg cm^{-2}	333.4 F g^{-1} (1 A g^{-1})	240 F g^{-1} (30 A g^{-1})	85.3% after 10000 cycles[9]
Hollow particle-based nitrogen-doped carbon	1.0 mg cm^{-2}	307.2 F g^{-1} (1 A g^{-1})	235.2 F g^{-1} (20 A g^{-1})	Not reported[10]
Nitrogen-containing mesoporous carbon	5.0 mg cm^{-2}	238.4 F g^{-1} (1 A g^{-1})	180 F g^{-1} (10 A g^{-1})	88% after 6000 cycles[11]
Hierarchically meso-/microporous carbon	2-2.5 mg cm^{-2}	163 F g^{-1} (0.5 A g^{-1})	129 F g^{-1} (50 A g^{-1})	90.3% after 10000 cycles[12]
Oxygen-enriched carbon	1.25 mg cm^{-2}	272.6 F g^{-1} (1 A g^{-1})	197 F g^{-1} (100A g^{-1})	100% after 10000 cycles[13]
Nitrogen-doped carbon	1.9 mg cm^{-2}	400 F g^{-1} (1 A g^{-1})	301.2 F g^{-1} (100A g^{-1})	100% after 10000 cycles[14]
Hierarchically porous nitrogen-doped carbon	1.1 mg cm^{-2}	497 F g^{-1} (1 A g^{-1})	287 F g^{-1} (30 A g^{-1})	92.8% after 10000 cycles[15]
Carbon nanocages	1 mg cm^{-2}	205 F g^{-1} (1 A g^{-1})	179 F g^{-1} (200 A g^{-1})	95% after 100000 cycles[16]
N- rich carbon arrays	**1.5 mg cm^{-2}**	**776.09 F g^{-1} (1 A g^{-1})**	**515.5 F g^{-1} (20 A g^{-1})**	**94.43% after 5000 cycles**
			316.8 F g^{-1} (100 A g^{-1})	
N- rich carbon arrays	**4.5 mg cm^{-2}**	**560.38 F g^{-1} (1.5 mA cm^{-2})**	**307.89 F g^{-1} (30 mA cm^{-2})**	**This work**

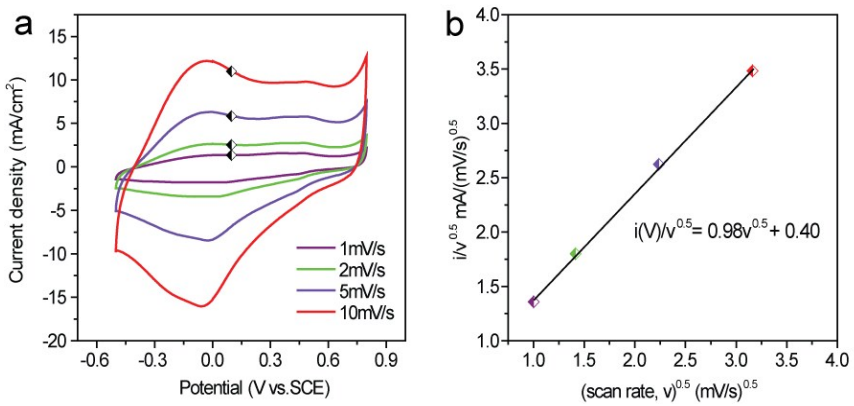

Figure S17 (a) CV curves of the NP350 electrode at four different scan rates. (b) i(V)/$v^{0.5}$ vs. $v^{0.5}$plot collected for NP350 using the anodic current at a potential of 0.1V vs. SCE.

Calculations in Dunn Method:

According to the Dunn method, the capacitance contribution can be divided into the capacitive controlled and the diffusion-controlled processes.[17] So, the current density at a fixed potential can be expressed as the combination of the above twoterms:[18]

$$i(V) = k_1 v + k_2 v^{0.5} \quad \text{(Equation S5)}$$

where $k_1 v$corresponds to the capacitive contribution, while $k_2 v^{0.5}$accounts for diffusion-controlled contribution. By dividing $v^{0.5}$ on both sides, the above equation can be transformed to the following form:

$$\frac{i(V)}{v^{0.5}} = k_1 v^{0.5} + k_2 \quad \text{(Equation S6)}$$

By plotting $\frac{i(V)}{v^{0.5}}$ vs. $v^{0.5}$, a linear fitting line is obtained with the slope k_1 and the y-intercept k_2.

Figure S17 displays an example of applying Dunn method to analyze the capacitive and diffusion-controlled contributions. At a fixed potential of 0.1V*vs*. SCE, the current density of each scan rate can

be obtained from the CV curves. After plotting $\frac{i(V)}{v^{0.5}}$ vs. $v^{0.5}$, the k_1 value of 0.98 can be obtained from the slope of the linear fitting line. Then the capacitive contribution was determined by $k_1 v$. The same process was performed for other potentials within the potential window. Finally, the ratio of the capacitive contribution in the whole capacitance can be draw out as the dark region in the blank region of Figure 3f.

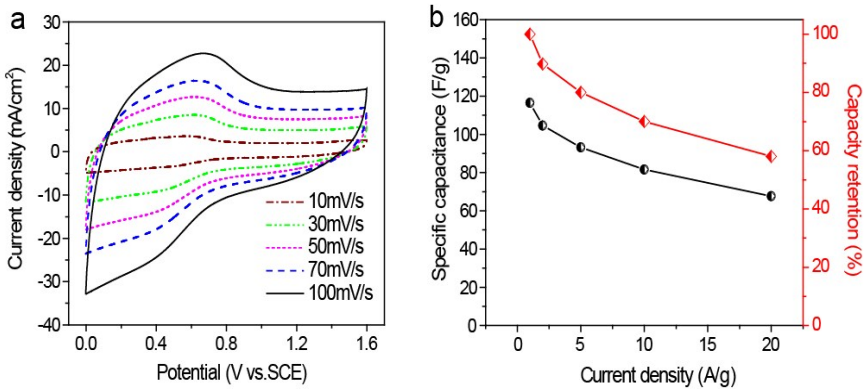

Figure S18 (a) CV curves of the device obtained at different scan rates. (b) Rate performance of the device at different current densities.

References

1. H. Peng, B. Yao, X. Wei, T. Liu, T. Kou, P. Xiao, Y. Zhang and Y. Li, *Adv. Energy Mater.*, 2019, DOI: 10.1002/aenm.201803665.
2. Q. Hao, X. Xia, W. Lei, W. Wang and J. Qiu, *Carbon*, 2015, **81**, 552-563.
3. Q.-F. Lü, Z.-W. He, J.-Y. Zhang and Q. Lin, *J. Anal. Appl. Pyrolysis,* 2011, **92**, 152-157.
4. L. Wang, Y. Ye, X. Lu, Z. Wen, Z. Li, H. Hou and Y. Song, *Sci. Rep*, 2013, **3**, 3568.
5. F. Zhang, T. Liu, M. Li, M. Yu, Y. Luo, Y. Tong and Y. Li, *Nano lett.*, 2017, **17**, 3097-3104.
6. T. Akhter, M. M. Islam, S. N. Faisal, E. Haque, A. I. Minett, H. K. Liu, K. Konstantinov and S. X. Dou, *ACS Appl. Mater. Interfaces*, 2016, **8**, 2078-2087.
7. K. Xiao, L.-X. Ding, H. Chen, S. Wang, X. Lu and H. Wang, *J. Mater. Chem. A*, 2016, **4**, 372-378.
8. S. Gao, X. Li, L. Li and X. Wei, *Nano Energy*, 2017, **33**, 334-342.
9. D. K. Kim, N. D. Kim, S.-K. Park, K.-D. Seong, M. Hwang, N.-H. You and Y. Piao, *J. Power Sources*, 2018, **380**, 55-63.
10. L.-F. Chen, Y. Lu, L. Yu and X. W. Lou, *Energy Environ. Sci.*, 2017, **10**, 1777-1783.
11. Y. Xu, J. Wang, Z. Chang, B. Ding, Y. Wang, L. Shen, C. Mi, H. Dou and X. Zhang, *Chem. Eur. J.*, 2016, **22**, 4256-4262.

12. J. Yang, H. Wu, M. Zhu, W. Ren, Y. Lin, H. Chen and F. Pan, *Nano Energy*, 2017, **33**, 453-461.
13. L. L. Zhang, H. H. Li, Y. H. Shi, C. Y. Fan, X. L. Wu, H. F. Wang, H. Z. Sun and J. P. Zhang, *ACS Appl. Mater. Interfaces*, 2016, **8**, 4233-4241.
14. T. Liu, T. Kou, D. Bulmahn, C. Ortuno-Quintana, G. Liu, J. Q. Lu and Y. Li, *ACS Appl. Energy Mater*., 2018, **1**, 5043-5053.
15. X. Wei, H. Zou and S. Gao, *Carbon*, 2017, **123**, 471-480.
16. Y. Bu, T. Sun, Y. Cai, L. Du, O. Zhuo, L. Yang, Q. Wu, X. Wang and Z. Hu, *Adv. Mater*., 2017, **29**, 1700470.
17. J. Wang, J. Polleux, J. Lim and B. Dunn, *J. Phys. Chem. C*, 2007, **111**, 14925-14931.
18. T. C. Liu, W. G. Pell, B. E. Conway and S. L. Roberson, *J. Electrochem. Soc.*, 1998, **145**, 1882-1888.